Modeling the Drying-Out of Mars

For submission to ROSES Solar System Workings 2018 (NNH18ZDA001N-SSW)

2. Scientific/Technical/Management.

2.1. Summary.

A record of Mars climate evolution is contained in shifts over time in the spatial distribution of evidence for rivers and lakes on Mars – in particular, the elevation+latitude distribution (Fig. 1; Kite 2019, Kite et al. 2019). **But the potential of this archive to constrain the atmospheric evolution of Mars is untapped, because our understanding of the effect of atmospheric pressure and greenhouse forcing on the elevation+latitude distribution of runoff on Mars is not adequate for this purpose.** A key control of surface liquid water potential on Mars is the pressure of the CO_2-dominated atmosphere ($P_{CO2} \approx P_{tot}$) (Wordsworth 2016, Haberle et al. 2017). While CO_2 alone cannot explain rivers and lakes on Early Mars, P_{CO2}(t) is nevertheless a key variable for providing a baseline of greenhouse warming, for suppressing evaporitic cooling, and for serving as a constraint on Mars atmosphere loss processes – and this is true irrespective of the nature of the needed non-CO_2 warming agent (e.g. Lammer et al. 2018, Ramirez & Craddock 2018, Haberle et al. 2017, Jakosky et al. 2018). For example, $P_{CO2} \gtrsim 10\times$ modern is thought to be required for wet climates on Early Mars (Ingersoll 1970, Jakosky et al. 2018, Hecht 2002). Indeed, so strongly does P_{CO2} affect Mars paleoclimate that changes in P_{CO2} between ~10 mbar and 1000 mbar are seen, in GCMs, to bring changes in the elevation and latitude distribution of both peak temperature, and snow/ice stability, which jointly control surface liquid water potential on Mars (Mischna et al. 2013, Kite et al. 2013, Wordsworth et al. 2015). (For example, high P_{CO2} is an essential ingredient of the Late Noachian Icy Highlands hypothesis; Head et al. 2017). The physical basis for this transition is clear: very thin atmospheres "[play] a small role for the heat budget of the surface" (Haberle et al. 2017), so (flat-)surface temperature is set by latitude alone. But, for a very thick atmosphere, winds even out latitudinal temperature gradients, and surface isotherms increasingly correspond to topographic contours. Thus, as P_{CO2} goes up, $\partial T_{surf} / \partial z$ becomes more negative (Wordsworth 2016). It is tempting to connect this effect with the shifts over geologic time shown in Fig. 1. **However, our current understanding of the effect of P_{CO2} on latitude and elevation distribution of rivers and lakes is too imprecise to be used to extract paleopressure constraints from the rock record (Fig. 2).** With improved P_{CO2} constraints, we can test the hypotheses that Mars dried up due to loss of its atmosphere (CO_2-Loss hypothesis) as well as the alternative endmember of loss of non-CO_2 greenhouse warming at constant P_{CO2} (Constant-Pressure Cooling). **Despite their opposing implications for the cause of Mars' drying-out, the Constant-Pressure Cooling and CO_2-Loss hypotheses have never been tested using the geologic record of Mars' drying-out; it is this gap that the proposed work will fill (Fig. 3).**

Thus, in order for the newly-synthesized geologic data (Fig. 1) to be used to constrain P_{CO2} change on Mars, there is a pressing need to improve our basic knowledge of the effect of P_{CO2} on the elevation+latitude distribution of surface liquid water potential (Fig. 2), and to apply that improved understanding to the drying-out of Mars (Fig 3). To this end, we will use an ensemble of general circulation model (GCM) simulations, varying orbital forcing, non-CO_2 greenhouse forcing, and other parameters, in order to determine (i) the causes of, and (ii) the key P_{CO2} values for, the effect of changing P_{CO2} on the elevation+latitude distribution of surface liquid water on Mars. Thus, we shall obtain both (1) basic estimates, and (2) a probabilistic look-up table, for the effect of P_{CO2} on the elevation+latitude distribution of rivers and lakes on Mars (Fig. 2). By comparing these to existing data on the elevation+latitude distribution of ancient rivers/lakes (Fig. 1; §2.4.3), we will obtain new constraints on P_{CO2} during ≥2 discrete geologic periods (Fig. 1). Finally, we shall combine our paleopressure record with existing constraints from other methods (e.g. Kite et al. 2014, Cassata et al. 2012, Manga et al. 2012).

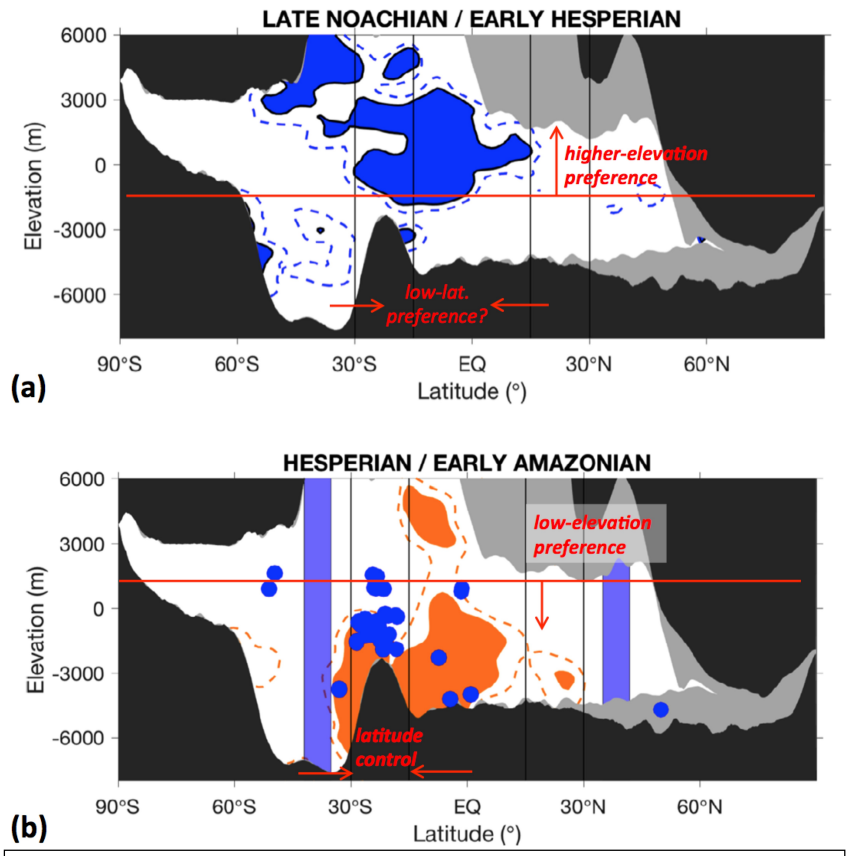

Fig. 1. Latitude-elevation plots of climate-relevant geologic activity for two periods of river-forming climate. The black regions have no data, and the gray regions correspond to terrain that was geologically reset after the time slice in question. Black lines: latitudes ±15° and ±30°. **(a) Late Noachian / Early Hesperian time slice:** Blue shading corresponds to the latitude/elevation zones that contain 67% of the valleys (Hynek et al. 2010), after correcting for the nonuniform distribution of latitude/elevation. **(b) Late Hesperian / Amazonian time slice:** Blue disks mark large alluvial fans (catalogs of Moore & Howard 2005 and Kraal et al. 2008a, total ~50 features). Pale blue stripes mark latitude range of Fresh Shallow Valleys (Wilson et al. 2016). We will recalculate this time slice as part of the proposed work (§2.4.3), using the 1500-feature database of Collaborator Morgan, which refines the basic trend shown here. Orange shading corresponds to light-toned layered sedimentary rocks (Malin et al. 2010), which are not part of this study. (This figure is based on Fig. 5 from Kite 2019).

2.2 Goal and objective of the proposed study.

The goal of the proposed work is to map and better understand the evolution of Mars' climatology and how it evolved from supporting an early wet environment to one which can no longer support liquid water. The objective of the proposed work is to obtain new constraints on Mars P_{CO2} during the Middle Noachian through Amazonian periods.

2.3. Scientific Background.

Better constraints on the cause of the drying-out of Mars are fundamental to the interpretation of discoveries from MRO, MSL, and MGS, as well as future observations of climate-relevant materials by ExoMars and Mars 2020. However, the relative contribution of **CO_2 Loss** (irreversible P_{CO2} draw-down) versus **Constant-Pressure Cooling** (i.e., loss of non-CO_2 greenhouse warming) to these changes is not currently understood (Fig. 3). These two divergent scenarios have very different implications for Mars climate evolution, the carbon cycle, and habitability at the outer edge of the Habitable Zone.

2.3.1. Data: Paleo-rivers that formed later in Mars history are found preferentially at lower elevations, and show a stronger dependence on latitude, relative to earlier rivers. These trends are not artifacts of preservation, but the physical cause of the signal is not known.

In the last few years, rich datasets for the distribution of precipitation-fed surface liquid water on Mars have been synthesized (reviewed in Kite 2019; Fig. 1). The new data allow surface liquid water activity to be divided into at least two time slices (Kite 2019 and references therein), with apparently different latitude and elevation preferences, suggestive of changes in P_{CO2} over time (Fig. 2). **But with only a vague and imprecise physical basis for relating these data to P_{CO2}, and many potential confounding factors (such as the strength of non-CO_2 greenhouse forcing, and orbital change), it is not clear what P_{CO2} history is (or histories are) consistent with these data.**

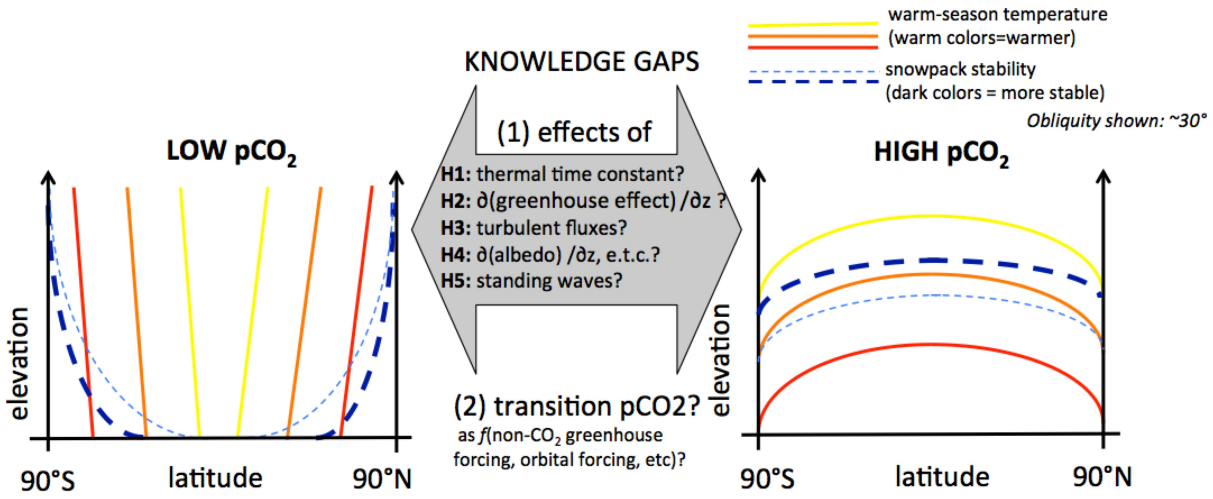

Fig. 2. P_{CO2} affects surface liquid water potential. At low pressure, warm-season temperatures track latitude bands but snow is most stable at low elevation (due to free-evaporitic convection), contrary to Earth-based intuition (Fastook et al. 2008, Kite et al. 2013, Wordsworth et al. 2013). At high pressure, both warm-season temperatures and snowpack stability track elevation bands, with differences (because snowpack stability responds to the annually averaged sublimation rate). Many effects contribute to this shift (gray box), and in the work described in §2.4.3 we will determine which is the most important.

A lot of the runoff on Early Mars came from rain/snowmelt (precipitation) (e.g., Malin & Edgett 2003, Howard & Moore 2005, Carr 2006, Malin et al. 2010, Kite 2019) (see Table 1 for how we will exclude features that are possibly groundwater-fed, impact-triggered, etc.). The existence of rain/snowmelt is a constraint on past climate. A wetter climate, with T_{surf} >0°C at least seasonally, is implied. A rain- or snowmelt-permitting climate very probably requires P_{CO2} > 6 mbar, because evaporitic cooling efficiently suppresses runoff at 6 mbar (Fig. 4; Hecht 2002, Mansfield et al. 2018). The distinct periods of river-forming climate show spatially more restricted fluvial erosion, and shorter rivers, with an overall trend to lower (planet-averaged) erosion rates, as the planet dried up (Howard et al. 2005, Kite 2019, Goudge et al. 2016, Golombek et al. 2014). Surprisingly however, intense, climate-driven runoff persisted late in Mars history, consistent with a major role for non-CO_2 greenhouse forcing (Kite et al. 2019a). **Relative to rivers that formed earlier in Mars history, rivers that formed later in Mars history were preferentially at lower elevation, and show a stronger dependence on latitude (Fig. 1). (This is after masking out resurfaced terrains for each time slice, correcting for terrain availability, and**

considering only nonglaciated terrains, i.e. it is not the result of preservation bias. The result is also not sensitive to the unusual preservation style of rivers in Arabia Terra). The nonuniform distribution of elevation as a function of latitude—for example, there is not much Noachian terrain south of 30°S above +3 km elevation—is corrected for in Fig. 1 using a kernel density estimator. For details of the refined correction we will use in the proposed work, see §2.4.3). These trends are consistent with previous reports, e.g., the elevation-controlled trends reported for the Middle Noachian (e.g. Craddock et al. 1993, Irwin et al. 2013), and the latitude trends reported for the Late Noachian / Early Hesperian valleys by Williams & Phillips (2001). Indeed, the spatial distribution of valley networks has been used to test warm/wet versus cold/dry hypotheses for Mars (Wordsworth et al. 2015, Bouley et al. 2016). For later materials, >¾ of large alluvial fans apices are at latitude 30° - 15°S (Kraal et al. 2008a), while Fresh Shallow Valleys are also confined to latitude belts (Mangold 2012, Wilson et al. 2016). **What is the cause of these shifts? Our work will advance the state of knowledge by improved modeling**, which is needed to quantify the effect of CO_2 loss, loss of non-CO_2 greenhouse forcing, and their combination on the observed latitude-elevation trends. **This modeling is crucial for reconstructing Mars P_{CO2} versus time and thus, the cause of the drying-out of Mars (Fig. 3).** For the first time, the proposed work would marginalize over the key uncertainties (orbital forcing, strength of non-CO_2 greenhouse effect), confront models with a dataset that has been corrected for preservation bias, and thus, constrain P_{CO2} versus geologic epoch.

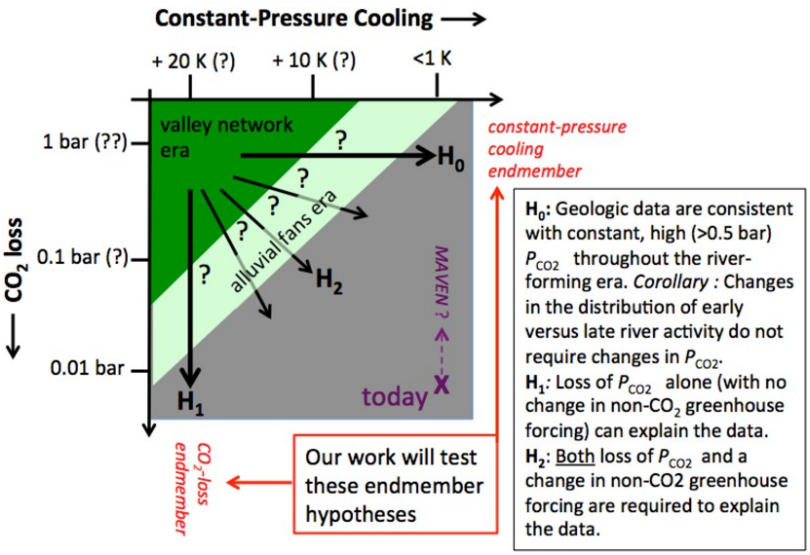

Fig. 3. Mars had rivers early in Mars history, but Mars is dry today. Although Mars has lost atmosphere over time, it is not clear if Mars late-stage rivers formed under high atmospheric pressure (**H_0**), or if late-stage rivers record atmospheric loss (**H_1**). Combining improved understanding of the effect of P_{CO2} on the elevation+latitude distribution of surface liquid water with geologic proxy data can constrain P_{CO2} versus time and thus constrain the drying-out of Mars.

2.3.2. Models: P_{CO2}'s effect on changes in the elevation+latitude distribution of surface liquid water is vital, but poorly quantified.

Latitude-Elevation plots are an underexploited unifying framework that pose a challenge to modelers: The data (Fig. 1) might be related to past climate, as follows. Latitude and elevation are key parameters for climate. Snow or ice will melt if they get warmed above 0°C. Insolation is the main control of snow temperature on modern Mars because the air is so thin. But for high P_{CO2}, exchange with the air can be the main control on T_{surf} (Wordsworth 2016). **There are several possible mechanisms for this and the relative importance of these mechanisms is – currently – unknown (Fig. 2).** One plausible hypothesis is as follows. Air temperature decreases with elevation, so at high P_{CO2}, turbulent fluxes ensure that T_{surf} also decreases with elevation

(Wordsworth 2016). Another likely contributor is that, at high P_{CO2}, greenhouse warming ($IR\downarrow$) becomes relatively more important (for all elevations), and $IR\downarrow$ is strongest at low elevation (Fig. 2). Other mechanisms also likely contribute (Fig. 2), and the relative contribution of these factors will be assessed as part of the proposed work. For whatever reason, at high P_{CO2} in GCMs, elevation and latitude are both important for determining T_{surf}. Snowpack stability also shifts with P_{CO2}, with a preference for ice-filled valleys at low P_{CO2} versus ice-capped mountains at high P_{CO2} (Fig. 4); models show that snowpack location is controlled by annual-mean sublimation rate (Fastook et al. 2008, Kite et al. 2013, Wordsworth et al. 2015).

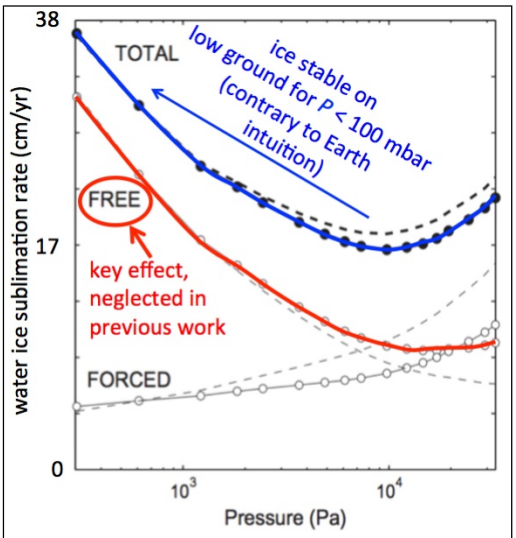

Fig. 4. Pressure dependence of diurnal-mean sublimation rate at an equatorial site. Free buoyant convection term dominates for P<~100 mbar. Dashed lines correspond to alternative parameterization of wind speed. (From Kite et al. 2013).

To sum up, the trends in Fig. 1 are consistent with theoretical expectations for **CO_2 Loss** (Wordsworth et al. 2013, Wordsworth 2016). Thus, combining data and theory hints that – during the Hesperian – P_{CO2} decreased. Although this hypothesis is exciting, it is currently both nonquantitative and nonunique: **an alternative scenario (Constant-Pressure Cooling) is that CO_2 pressure varied little *during* Mars' wet era, but the strength of non-CO_2 greenhouse forcing waned.** This alternative hypothesis is reasonable because it is known that CO_2 alone is not enough to generate a lake-forming climate (Fig. 3), so both CO_2 and non-CO_2 greenhouse warming are needed to explain rivers and lakes on Early Mars (e.g., Turbet and Tran 2017). In this alternative scenario, early on, temperatures were high everywhere but snow/ice was located at high ground (cold traps), so melting was confined to high ground. Later on, temperatures had dropped so that $IR\downarrow$ (which is strongest at low elevations) was the limiting factor for patchy low-elevation melting. In this alternative scenario, the latitude preference is explained by appealing to unusual orbital conditions as the trigger for melting, because unusual orbital conditions can favor certain latitude belts (Mischna et al. 2003, Kite et al. 2013). **Despite their oppposing implications for the cause of Mars' drying-out, the Constant-Pressure Cooling and CO_2-loss hypotheses have never been tested for the geologic record of Mars' drying-out; it is this gap that the proposed work will fill.**

Because these are intrinsically 3D hypotheses, we will use a GCM (MarsWRF), altering P_{CO2}, non-CO_2 greenhouse forcings, orbital parameters, etc., and tracking both T_{surf} (>0°C vs. <0°C) and the relative stability of snow and ice as functions of elevation+latitude. As shown by Wordsworth et al. (2013), high P_{CO2} causes snow and ice on Mars to migrate to high elevation, so high elevations are favored for snow-melt at high pressure. However, neither the causes of this shift, nor the conditions under which it occurs, have been investigated in sufficient detail (Fig. 2). For example, many paleo-Mars GCMs do not include the free buoyant convection contribution to sublimation, but this effect is known (Ingersoll 1970, Hecht 2002; Fastook et al. 2008, Kite et al. 2013; Mansfield et al. 2018) to be critical to the shift from the most melt-prone gridpoints being at low elevation, to the most melt-prone gridpoints being at high elevation. Indeed, free buoyant evaporitic cooling is the dominant term for any possible $H_2O_{(l)}$ exposed at the surface of Mars today (~80% of total energy loss; 10× more important than forced evaporitic cooling; Fig. 4). (To

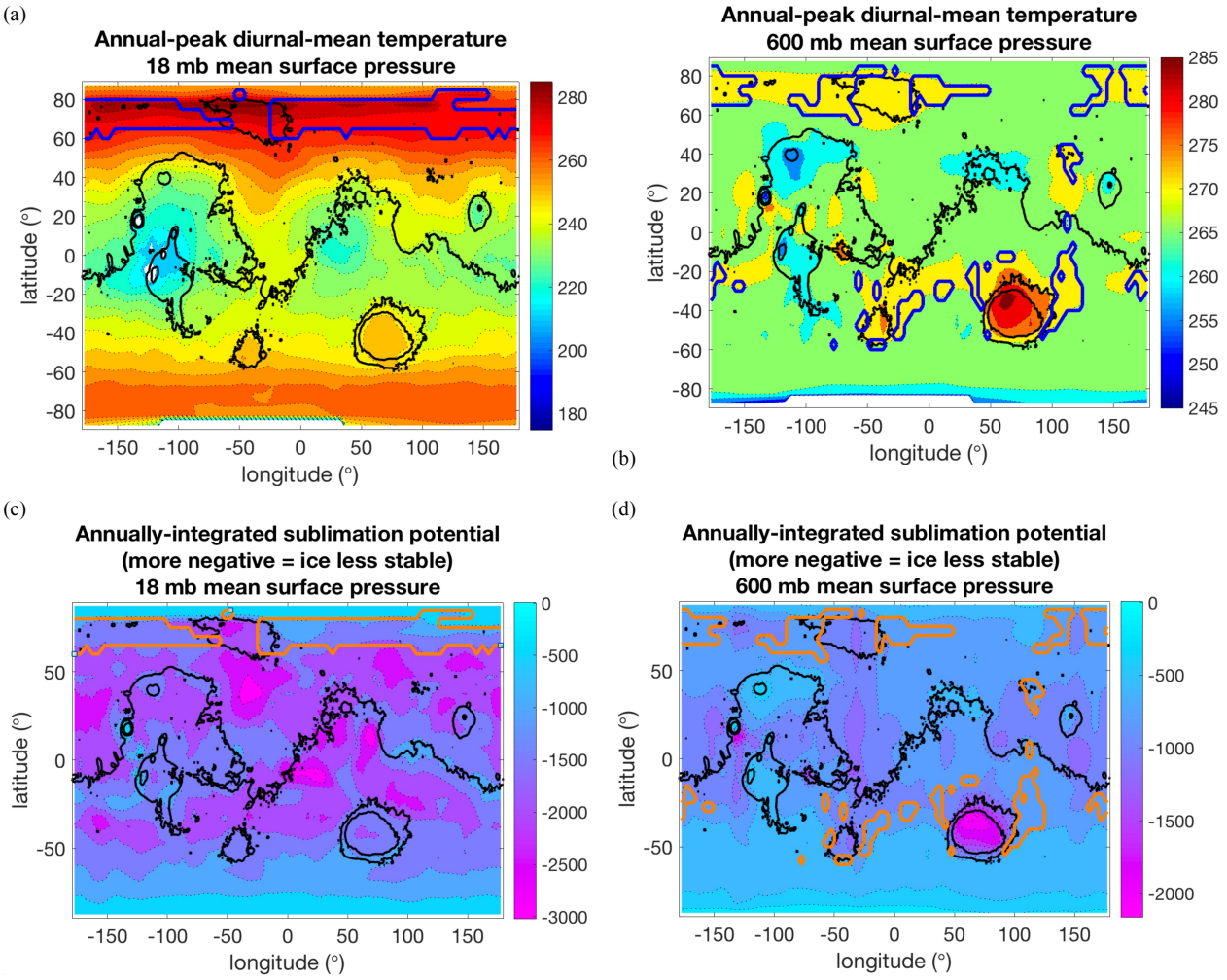

Fig. 5. Preliminary MarsWRF run output, illustrating the core physical effect to be investigated by the proposed work. (a) Seasonal-peak temperatures, 18 mbar: mostly latitudinally-controlled, with some effect from dust continents. (b) Seasonal-peak temperatures, 600 mbar: latitude effects relatively minor. (c) Snowpack potential sublimation map (annually integrated sublimation rate of snow, had snow been present at each gridpoint), 18 mbar. Snow relatively stable at low elevations along dichotomy boundary. (d) Snowpack stability map (annually integrated sublimation rate of snow, had snow been present at each gridpoint), 600 mbar. Snow unstable on low ground. Obliquity 25°, eccentricity 0.1 for the runs shown. In all panels, thin black solid lines are MOLA topography. Thick colored solid lines outline melt zone. Note: Because our GCM does not yet include gray gas parameterization, Early Mars runs produce no melt. Therefore, we increased the solar luminosity to 90% of modern in these illustrative runs in order to demonstrate our melt-zone identification procedure.

be clear, this omission does not invalidate previous GCM work, which has either $T_{surf} \ll 273$K or >300 mbar P_{CO2}. But it does prevent exploration of melt-prone low-P_{CO2} climates, which are a focus of the proposed work). **Thus, previous work has a snow-to-high-ground bias for melt-prone climates, and we will advance the state of the art by removing this bias.**

2.3.3. Combining improved models of the effect of P_{CO2} on the elevation+latitude distribution of surface liquid water potential with existing data can constrain P_{CO2} versus time and thus the drying-out of Mars.

Given that the importance of P_{CO2} change to early Mars climate has been noted for more than 40 years (Sagan et al. 1973, Haberle et al. 2017), it is perhaps surprising that there is no systematic study of the effect of P_{CO2} on the spatial distribution of surface runoff potential on Early Mars, the closest being Fig. 10 in Wordsworth et al. 2015. (Both Richardson & Mischna 2005 and Kite et al. 2013 consider the effect of P_{CO2} change on transient diurnal pulses of liquid water, which are sufficient to wet soil. However, diurnal-average temperatures above 0°C are likely needed to avoid meltwater refreezing and explain the river runoff implied by dry-river beds; Clow 1987, Kite et al. 2019. Diurnal-average temperatures above 0°C are much more challenging to achieve in CO_2+H_2O GCMs, which is part of the motivation for our gray gas approach) (§2.4.1). To assess and confirm the likely consequences of P_{CO2} changes, we carried out preliminary work with the MarsWRF GCM. Our results broadly reproduce the results of Wordsworth et al. 2015's Fig. 10. This confirms that differences in the details of the GCM do not alter the basic "high P_{CO2} = ice-at-high-ground" result reported by Wordsworth et al. (2013).

2.4. Technical Approach and Methodology.

Achieving our objective (§2.2) involves the following steps:

Step 1. (~85% of effort). Use a grid of >200 runs of the MarsWRF GCM improved by adding a gray gas, in order to determine (i) the causes of, and (ii) the key transition pressures for, the effect of changing P_{CO2} on the elevation+latitude distribution of surface liquid water on Mars (§2.4.1/2)
Step 2. (~15% of effort). Compare to the elevation+latitude distribution of past rivers to constrain both P_{CO2} , and non-CO_2 greenhouse forcing, for ≥3 different epochs (§2.4.3).

In order to define a focused, well-posed investigation of appropriate scope for a three-year study, we make several simplifying assumptions, which are explained and justified in §2.4.4.

Our proposed work will build on consensus ideas in atmospheric dynamics and Mars global climate modeling, and advance the state-of-the-art by refining these ideas and combining them with basic geologic constraints. Two features of the problem greatly reduce the computational burden and enable the proposed science. (1) Our previous experience studying orbital forcing (e.g. Mischna et al. 2013; Kite et al. 2013; Mansfield et al. 2018) has identified (only) 5 key orbital states that span the range of effects of orbital forcing on runoff potential. (2) Snow and ice tend to pile up where sublimation is minimized, and (at any one time) liquid water is volumetrically minor compared to the ice reservoir (Wordsworth et al. 2015, Mischna et al. 2003, Kite et al. 2013). Therefore, we can run the GCMs without interactive melt handling, and allocate surface liquid water potential flexibly in postprocessing. Our overall strategy is as follows (for detail, see §2.4.2). (1) Add a gray gas absorber to the MarsWRF GCM. (2) Using the gray gas enhancement, build an ensemble of GCM predictions of peak diurnal T_{surf} as a function of P_{CO2} and gray gas absorption, also varying orbital parameters. We will also separately improve understanding of how and why the elevation-dependence and latitude-dependence of surface temperature changes as with increases in P_{CO2} via runs with idealized boundary conditions (for example, simplified topography runs). Our analysis of these runs will provide mechanistic insight (which factors matter the most, and which do not?) (3) Compare the improved model with data to get improved P_{CO2} constraints for 2 or more time slices. Specifically, we will integrate with data to produce P_{CO2} constraints for two time slices, Late Noachian / Early Hesperian and Late

Hesperian / Amazonian (Table 1). This will give a geologically-based estimate of whether or not the atmospheric pressure dropped during the Hesperian, a times of great interest for Mars rivers, using the distribution of the rivers themselves.

2.4.1. Description of the Mars GCM, including proposed refinements.

We shall use co-I Mischna's early-Mars-optimized version of the MarsWRF (Mischna et al. 2013) Mars GCM. MarsWRF is a version of the PlanetWRF GCM (Richardson et al. 2007), itself derived from the terrestrial mesoscale Weather Research and Forecasting (WRF) model (Skamarock et al. 2005). We will run MarsWRF with horizontal resolution of 5.625° in longitude and 3.75° in latitude. The vertical grid uses a modified-σ (terrain-following) coordinate system with 53 vertical resolution levels. CO_2 radiative transfer uses a correlated-*k* scheme spanning 0.4-1000 μm (Mischna et al. 2012). The surface layer flux parameterization scheme is a Monin-Obukhov scheme, i.e., the critical free buoyant convection term (Fig. 4) is already included in the model (Pielke et al. 2002). The co-I is a developer of the model, and the PI is an experienced user of the model. The proposed work is actually simpler than what has been done in our already-existing collaboration (e.g., Kite et al. 2019b). Therefore, the proposed work has low technical risk. The only planned refinement to the model is the addition of a gray gas capability to MarsWRF. The gray gas shall have zero absorption coefficient below 4.5 μm and an adjustable, constant absorption coefficient above. A central aim of our study is to decouple the effect of loss of CO_2 from the effect of non-CO_2 greenhouse warming. To simplify this, we will pick the value of κ (m^2/kg) in order to produce a specified additional (non-CO_2) infrared optical depth, τ, at reference elevation (0 m). Although the notation differs, this will still allow easy comparison to previous work using gray gases (e.g. Palumbo & Head 2018). The addition of this gray gas to MarsWRF is straightforward, requires minimal modification of the radiative transfer code, and no additional derivations of absorption coefficients. Several processes in MarsWRF (such as Rayleigh scattering) are treated as quasi-gray (i.e., the value is uniform within each of MarsWRF's 14 spectral bands), and so MarsWRF has already been designed to handle additional gray gases. Incorporating a new gray gas to the model requires only assignment of the absorption coefficient of the gas to each spectral band. The value of the gray gas absorption is chosen at runtime through a namelist file, and only minor plumbing is necessary to introduce the required additional calculations.

2.4.2. Detailed description of model runs and analyses to be performed.

Our runs will have two purposes, and will be divided into two overlapping sets: **Set A:** (~50 runs) Test hypotheses for coupling between $\partial T_{surf} / \partial z$ and atmosphere lapse rate (Fig. 2). **Set B:** (~200 runs) Constrain P_{CO2} versus time.

Set A: (~20% of runs). Here our goal is to use MarsWRF to understand a physical process that is generally relevant to worlds with a solid surface and some atmosphere. Therefore, we will make idealizations to get a process understanding. Most runs will be for a seasonless orbit, with zero obliquity, uniform thermal inertia (250 SI units), uniform albedo (0.25), negligible dust loading,

Fig. 6. Overview of ensemble approach.

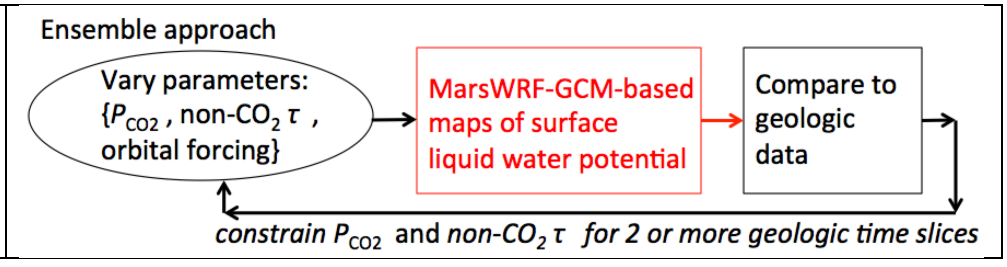

and no CO_2 condensation and no $H_2O_{(v)}$. We will consider both MOLA (M) and Cosine (C+,C-) topography. {C+,C-} shall be defined by elevations that are a function of the cosine of latitude (only), with a half-amplitude of 2 km. C- will have maximum elevation at the poles and C+ will have maximum elevation at the equator. The half-amplitude is chosen so as not to greatly affect the general circulation (Richardson & Wilson 2002, Zalucha 2006), while still allowing $\partial T_{surf} / \partial z$ to be diagnosed. Basic model set-up will be as §2.4.1. Set A runs will be as follows:

BASELINE: Runs at{6, 60, 120, 200, 400, 600, 1200, 2400} mbar for {M,C+,C-} topography (Total: 24 runs), at present-day solar luminosity. By interpolation (for each topography), we will define the "transition pressure" (P_{trans}) as the P_{CO2} for which $\partial T_{surf} / \partial z$ is half-way between $\partial T_{surf} / \partial z$ at 6 mbar and 2400 mbar.

We describe the rest of simulation Set A in terms of a series of hypothesis tests. **H1:** "The shift in $\partial T_{surf} / \partial z$ is mainly (>50%) the result of an increase in the thermal time constant of the atmosphere relative to the surface thermal time constant." Test: Increase surface thermal inertia 10-fold while holding all other parameters constant. If P_{trans} rises by less than a factor of 2, H1 is falsified. (2 runs bracketing P_{trans} for each of 3 topographies = 6 runs). **H2:** "The shift in $\partial T_{surf} / \partial z$ is mainly (>50%) due to an increase in the importance of the greenhouse effect at high P_{CO2}". Test: Set the absorption coefficient of CO_2 to zero. If $\partial T_{surf} / \partial z$ at high P_{CO2} does not decorrelate with elevation, or if P_{trans} rises by less than a factor of 2, H2 is falsified. (2 runs bracketing P_{trans} for each of 3 topographies = 6 runs). **H3:** "Because of Mars' strong day-night temperature cycle, timescales matter. Therefore, the value of P_{trans} will depend on the details of turbulent flux exchange with the surface." Test: Reduce surface roughness from a uniform value of 0.03 m (the default; based on Mars Pathfinder data; Sullivan et al. 2000) to 0.0001 m (appropriate for smooth dust plains or glacier ice). If P_{trans} is the same within 20%, then H3 is falsified. (2 runs bracketing P_{trans}, only for MOLA topography = 2 runs). **H4:** "On Mars, high albedo + low-TI dust continents are on high ground, which should affect $\partial T_{surf} / \partial z$ significantly." Test: In order to quantify the effect of dust continents, we will run (i) with actual Mars albedo and actual Mars TI (ii) with actual Mars albedo, but uniform TI, (iii) with uniform albedo, but actual Mars TI; and compare to runs with uniform albedo and Mars TI (3 × 2 runs bracketing P_{trans}, MOLA topography, compared to runs from BASELINE). **H5:** "The complexities of Mars' general circulation, which are forced by topography, cannot be disentangled from $\partial T_{surf} / \partial z$ nor from $P_{trans.}$" H6 can be tested by comparing the BASELINE(M) runs (real Mars topography) to the BASELINE(C+,C-) runs, which have much more subdued topography. If neither $\partial T_{surf} / \partial z$ nor P_{trans} differ by more than 33%, then H6 is falsified. **Total:** 24 BASELINE + 20 hypothesis-test runs = 44 runs ≈ 176,000 CPU-hours.

Several additional metrics for comparison shall be output and analyzed for the purpose of understanding controls on $\partial T_{surf} / \partial z$, as follows. (i) Global area-averaged lapse rate in annual-mean surface temperature. (i) Global area-averaged lapse rate in warm-season surface temperature. (iii) <40° |latitude| lapse rate in warm-season surface temperature. (iv) 2D regression of annual-mean surface temperature on latitude and elevation. (v) 2D regression of warm-season surface temperature on latitude and elevation.

Set B: (~80% of runs). Here our goal is to connect to geologic proxy data, which dictates greater realism and careful tracking of uncertainties. Runs will be carried out for 8 values of atmospheric pressure {6, 60, 120, 200, 400, 600, 1200, 2400} mbar, 5 combinations of orbital parameters {45° obliquity, e = 0.093, L_p = 251°, which are the modern values; 45° obliquity, otherwise

present-day; 25° obliquity, L_p = 71°; 45° obliquity, L_p = 71°; and 45° obliquity, L_p = 0°, e = 0.12, which is optimal for melting according to Kite et al. 2013}, 5 values of τ {0, 0.5, 1, 2, 4, 10}. In order to reduce the number of τ runs, we will exploit the fact that runs that do not predict surface liquid water cannot match the geologic data. We will do this in the following way. For each orbital-parameter/P_{CO2} combination, we shall start with high-τ runs and move down in τ until no surface liquid water is predicted, and not run the GCM for any lower values of τ for that combination. We shall carry out 1 true polar wander sensitivity test using the paleopole of Citron et al. (2018), and 2 sensitivity tests with changed (70% and 90% of modern) solar luminosity. **Total: <**200 runs ≈ <800,000 CPU-hours. The selected combinations of orbital parameters have proven to span the range of behavior in terms of the spatial distribution of surface liquid water potential based on previous work (e.g., Kite et al. 2013). The P_{CO2} / τ mesh is densest in the area where we anticipate thresholds in surface liquid water potential will occur based on prior publications; if this turns out not to be the case based on initial endmember-case runs, we shall adjust the mesh to track the newly interpreted thresholds.

Dust will be set to negligible opacity values, which maximizes T_{surf}. We will run with a CO_2 cycle including CO_2 ice clouds, and CO_2 seasonal polar cap condensation. $H_2O_{(v)}$ will be radiatively active, with a constant relative humidity of 0.1 (Mischna et al. 2013). Each run will be for 7 years which allows ample time for spin- up. Thermal inertia and albedo will be spatially uniform and equal to the modern average values, and solar luminosity will be 471 W/m^2 (78% of modern) (§2.4.4). Runs will be initialized without surface $H_2O_{(i)}$.

The last two years of the run will be averaged in subsequent calculations, except in cases where atmospheric collapse is clearly occurring, in which case we will note that atmospheric collapse is occurring but not otherwise use the output from that run. GCM output will be sampled at 520 points during the last 2 Mars years (approximately once every 2.5 sols) which provides a good sampling of times-of-day and of seasons. The GCM calculations are computationally intensive and require intensive use of a cluster (see F&E), but all subsequent steps are computationally inexpensive and can be carried out on a desktop computer.

The results will be post-processed in GrADS to produce maps of annual-peak diurnal-mean temperature (which will be not much less than the warmest-month temperature) and of annually integrated water ice sublimation potential (i.e. total water ice loss rate had ice had been continuously present during the year), using the equations of Dundas et al. (2010) as implemented in Kite et al. (2013). The movement of water ice under obliquity change is relatively well understood based on geology (Head & Marchant 2014) and models (e.g. Kite et al. 2013, Wordsworth et al. 2015), with the main finding being that water ice accumulates year-on-year in areas that minimize the year-averaged water ice sublimation rate. These two maps will be aggregated (two sets of 200 maps), and then interpolated in MATLAB using log-linear interpolation in P_{CO2} and κ in order to densify the mesh.

Finally, the maps will be converted into maps of surface liquid water potential (example: colored outlines in Fig. 5). To do this, we will take the seasonal-mean diurnal average temperature, and threshold at 273K (T_{surf} > 273K scores 1, T_{surf} ≤ 273K scores 0). We will then marginalize over the surface snow coverage fraction (based on rank in the areal snow coverage map) by summing the product of the thresholded temperature map with a range of areal snow coverage fraction (assigned based on rank in the favorability-for-snow-accumulation maps) from 1% (present-day value) up to 30% (most extensive snow cover predicted by GCMs), using a log-uniform prior.

Thus, a gridpoint that is above 273K, but is in a location very unfavorable for snow accumulation (e.g. 31%), will score zero on this combined map. (Maps of areas with $T > 273$K with no snow stability cutoff, which corresponds to likelihood of rainfall runoff, will also be propagated through all subsequent steps). We will also interpolate the resulting probability of surface liquid water onto an 8 pixel-per-degree MOLA MEGDR grid, i.e. taking account of the effect of elevation variations on local temperature, assuming a constant scale height of 10.7 km. This resolves craters with large elevation ranges (e.g. Gale) for model-data comparison. The result will be un-normalized maps of relative surface liquid water potential. **Thus, the results from Set B shall explicitly relate Mars surface liquid water potential to the two hypotheses of Constant-Pressure Cooling and CO_2 Loss.** Our next step will be to test these hypotheses against data.

2.4.3. Confronting the CO_2-loss hypothesis with geologic data.

Time Slice	**Late Noachian / Early Hesperian**	**Late Hesperian / Amazonian**	***Youngest fans/deltas***
Input Data	Valleys and valley networks	Precipitation-fed subset of young fans and deltas	
Source	Public USGS Hynek et al. (2010) dataset	Collaborator Morgan's database (Morgan et al. 2018)	
Age control	Crater counts (Fassett & Head 2008, Hoke & Hynek 2009)	Morphology of host crater (e.g. Mangold et al. 2012)	*Crater counts (Fig. 7)*
Preservation Mask (To Be Excluded)	Tanaka et al. 2014 units containing "A" or "lH"; |(latitude) | >40°; valleys on or near volcanoes	Tanaka et al. 2014 units containing "lA";| (latitude) | >40°	
Other Preservation Complexities, Exceptions/ Exclusions	Arabia Terra removed due to unusual preservation style (Davis et al. 2016). Exclusions: Outflow channels, valleys near volcanoes, Hesp./Amaz. valleys	Late Hesperian / Amazonian fans are generally easily identifiable. (Morgan et al. 2018). Exclusions: Possibly groundwater-fed features (e.g. Hauber et al. 2013); possibly impact-triggered fans (e.g. McEwen et al. 2007, Williams & Malin 2008, Goddard et al. 2014); gullies & RSL (Dundas 2017a, 2017b); fans catalogued as "small, debris-flow fans"; fans <10 km^2 in area; and fans with CTX confidence level <3.	
Numerator for areal density calcs.	(1) # of valley networks (2) combined length of valleys	Fan/delta area, normalized to area of host craters.	

Table 1. How existing data syntheses will be adapted for comparison with models.

The data we need are already in hand (Fig. 1). The overall workflow for each time slice[1] is to bin the data in 2D latitude-elevation boxes (10° × 2000 m, which gives a good balance between resolving shifts over time versus statistical significance); divide (bin-by-bin) by the area on which paleo-surface-liquid water evidence could plausibly be preserved in order to get a feature density per unit area including bootstrapped error bar; normalize by the planet-integrated feature density for that time slice; and cross-correlate each time slice with the probabilistic surface liquid water potentials for each model for each 2D bin. **The result will be a goodness score for each of the GCMs for each time slice, and we will take the best-fit from the 5 orbital forcing cases to get a 2D goodness score for each combination of (P_{CO2} + non-CO_2-greenhouse warming) for each time slice.** We choose to take the best-fit orbital forcing because the cumulative duration of runoff is consistent with runoff occurring only during orbital optima (e.g. Moore & Howard 2005, Kite et al. 2019).

Table 1 shows details of this process. For the Late Hesperian / Amazonian analysis, we will use fan/delta area, normalized to interior-to-crater area, as a proxy for the intensity of precipitation-driven erosion. This choice represents a trade-off between using the number of fans (which over-

[1] This workflow yields more statistically rigorous error bars than the kernel density estimation procedure used to make Figure 1.

weights the numerous small fans) and using fan volume (which would require building and analyzing hundreds of CTX DTMs).

We shall gauge uncertainty on the resulting best-fit in 4 ways. (1) Formal error will be obtained by bootstrapping the data (on a per-VN basis for Hynek et al. 2010, and a per-host-crater basis for Morgan et al. 2018). This is useful because no Mars histories that agree with the best-fit within formal error can be rejected. Mars histories that diverge greatly from the best-fit are disfavored and may be rejected. (2) We will separately cross-correlate data and models in latitude-longitude bins, and in latitude-elevation bins. To the extent that different models are favored based on choice of coordinates, that will be a flag that the longitudinal variations are important. (3) Sensitivity to the different definitions of density, and surface liquid water evidence, in Table 1. (4) Geological 'sanity check'. We will determine if the best-fit selection clearly depends on a geological site (or sites) that, in the judgement of the PI considering the advice of the Collaborator, is (are) anomalous. If so, the fit will be repeated with the anomalous site (or sites) removed, and the results for both fits shall be reported.

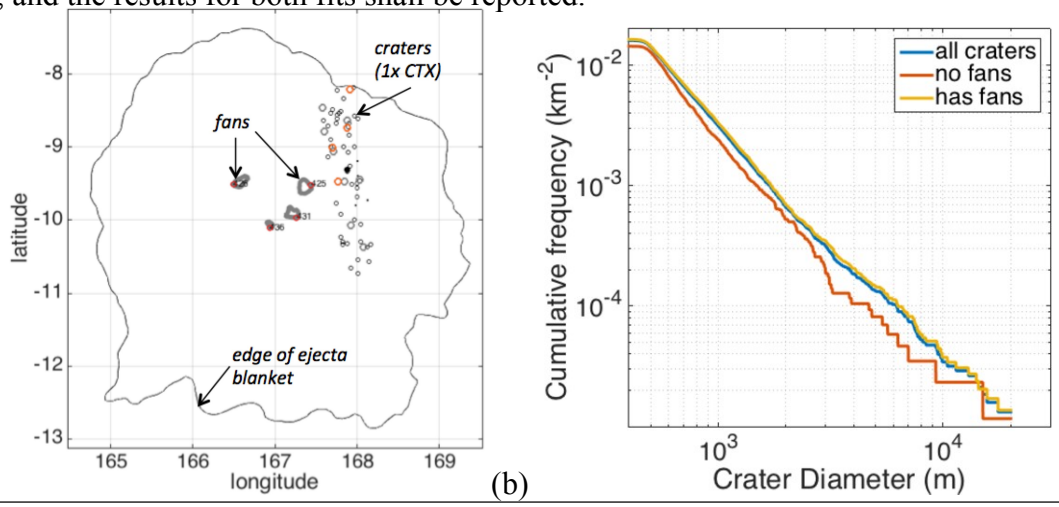

Fig. 7. (a) One of the 126 ejecta blankets for which we have already gathered data, which in combination with the models to be developed in the proposed work, will help to constrain the paleopressure evolution of Mars. (b) Cumulative crater size-frequency distribution (n = 6076) for all blankets, showing completeness down to 500m and an offset in age between no-evidence-for-fluvial activity craters ('dry'), which are, on average, younger, and with-evidence-for-fluvial-activity craters ('wet'), which are, on average, older.

Going from 2 to 3 time slices: capturing the end-game for river erosion on Mars.
Although getting P_{CO2} constraints for 2 time slices would be sufficient to achieve our goal and our objective, a modest additional calculation will add further value to the investigation by adding a third time slice. Specifically, we have already carried out a crater count on 126 separate ejecta blankets mapped as "Amazonian and Hesperian impact unit" (AHi, yellow) in the Tanaka et al. (2014) geologic map for |lat.| < 40°. The combined counted area is 3.8×10^5 km^2 (the threshold for meaningful crater-age dating is ~10^3 km^2; Warner et al. 2015). ~30% of these ejecta blankets encircle craters that have evidence for climate-driven river erosion (Collaborator Morgan et al. 2018), excluding impact-triggered runoff; Mangold et al. 2012b). In order to identify the distribution of fans for the last stages in river erosion on Mars's surface, we will sort the ejecta blankets into two bins based on N(0.5 km) cumulative crater density: one containing the fan-hosting craters with relatively young age, and the other containing the fan-hosting craters that have relatively old age. Poisson statistics ensure that some young ejecta blankets will have many

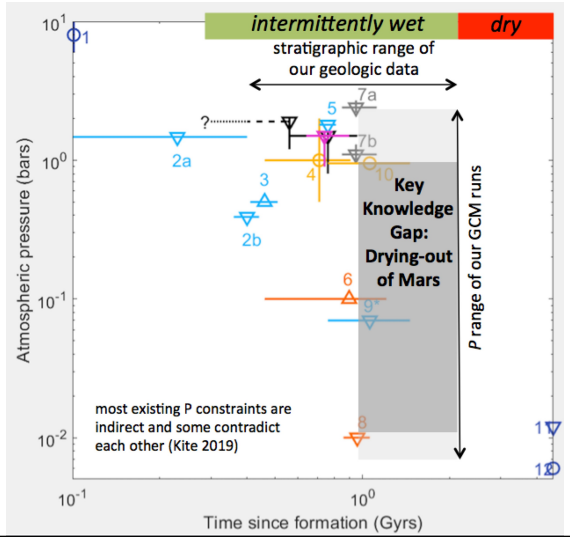

Fig. 8. (modified after Kite 2019). Our proposal in the context of (a small subset of) published atmosphere evolution reconstruction studies, showing that the proposed work is a natural extension of long-standing community-wide efforts towards constraining the P_{CO2} evolution of Mars. **Note the paucity of constraints between the Late Noachian and today, a key gap that will be addressed by the proposed work.** Numbers refer to different existing constraints from Kite (2019), but are not important in this context.

craters and vice versa, and the ejecta-blanket age only gives an upper limit on the age of the fans/deltas within the crater. Nevertheless, in aggregate, the large count area ensures that the set of low-crater-density craters will have a younger average age. Indeed, this method has been shown to yield coherent results (Wilson et al. 2016). Repeating the Table 1 workflow, we will identify (a) the approximate timing of final dry-out of Mars' |lat.| < 40° surface, (b) the geographic locations of the last pulse of river-forming climate on Mars, and (c) the P_{CO2} + non-CO_2-greenhouse warming required to explain the last pulse of river-forming climate on Mars. Finally, we will compare our paleopressure constraints to existing paleopressure constraints (e.g. Fig. 8) and determine whether or not a single history is consistent with all data.

2.4.4. Assumptions and caveats

It is worth emphasizing the limitations and assumptions of these modeling methods. (1) Our method cannot detect pressure changes within the range <10 mbar nor within the range ≳1 bar. This limitation is (fortunately) not germane, because the range of uncertainty for Early Mars atmospheric pressure (~0.01-1 bar; Hecht 2002, Kite 2019) is in the range where current GCMs say our technique will be most sensitive. (2) It is possible that the shift in river distribution requires not just loss of non-CO_2 greenhouse warming (H_0 in Fig. 3), nor just atmospheric decay (H_1 in Fig. 3), but rather a combination of the two (H_2 in Fig. 3). This would still be an interesting result. (3) It is possible that the atmosphere spends most of the time collapsed, and the rivers/lakes only record the inflated intervals (Soto et al. 2015, Kite et al. 2017c). In that case, our results will still constrain the atmospheric pressure at times when Mars climate supported rivers and lakes, so this is not a severe limitation. (4) Our modeling approach neglects mesoscale processes (e.g., orographic precipitation, steep slopes). Since no one has investigated the global trends before, we chose to start with a global modeling approach; we have published a paper applying slope effects in post- processing (Mansfield et al. 2018), so can investigate this if the output merits it. The drying-out of Mars had a long and presumably complex history; we propose to test simple hypotheses about that history, with an eye to enabling richer hypotheses and tests in the future.

In addition to these limitations, there are other potential concerns that are fully addressed/mitigated by our technical approach. These include: *T_{surf} will be overestimated due to lack of evaporitic cooling.* Response: This can't change gridpoint ranking (preferred snow locations), but does mean that T_{surf}> 273K zone will be a be slightly wider than in reality, so best-fit κ will be slightly underestimated. This minor penalty is accepted due to the large CPU-hour

savings. *Polar wander?* We will carry out a polar wander sensitivity test, using the best-estimate paleopole (Citron et al. 2018). If large-amplitude polar wander did occur, then this will show up in our maps as a 180° wavelength 'twist' in data relative to models (Bouley et al. 2016), enabling recalculation. *Neglect of Solar brightening by ~5% from 3.8 Ga to 3.0 Ga.* We will carry out sensitivity tests at 90% and 70% of modern solar luminosity. Moreover, insolation trades off with gray gas absorption coefficient (Govindasamy and Caldeira 2000, Caldeira et al. 2013). Thus, insolation error will bias best-fit τ, but not P_{CO2}. *How can a well-mixed gray gas be representative of all non-CO_2 greenhouse forcings? Clouds, for example, are not well mixed horizontally.* A well-mixed gray gas with adjustable absorption coefficient can approximate the effect of many potential non-CO_2 Mars warming agents (e.g. H_2, Tosca et al. 2018, and CH_4, Kite et al. 2017, Ramirez 2017). Although cloud coverage on Earth is far from complete, Ramirez & Kasting 2017 show that water ice cirrus clouds can only provide strong greenhouse warming on Early Mars if cloud coverage is close to complete. *How can you track snow/ice if there's no water ice in the model?* We use the potential-well approximation (Kite et al. 2013), which has been confirmed to work in a GCM (Wordsworth et al. 2015). *What about rain (not snowmelt)?* Maps of T_{surf} > 273K (rain-prone gridpoints) will be propagated and analyzed.

2.5 Perceived Impact of the Proposed Work.

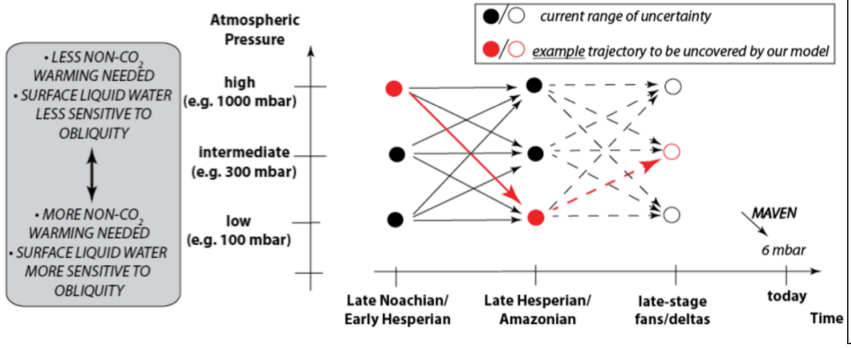

Fig. 9. Our modeling will enable improved understanding of P_{CO2} versus time. The dashed lines correspond to a new time slice that we will add in §2.4.3.

The proposed work will develop a new proxy for climate change *during* the wet era of Mars (Fig. 9). So far, effort has focused on climate change *between the wet era and the present day* (Haberle et al. 2017; Fig. 3) The proposed work will apply an improved knowledge base to a basic unexplained pattern in the Mars geologic record. Specifically, the competing **CO_2 Loss** and **Constant-Pressure Cooling** hypotheses **can be tested with existing data** by combining constraints from an ensemble of GCM simulations. **The new angle on Mars P_{CO2} history offered by the elevation+latitude distribution of Mars paleolakes and rivers is sorely needed:** high-profile P_{CO2} estimates published in the last 3 years vary by 2 orders of magnitude. For example, Lapôtre et al. (2016) suggest <10 mbar, Haberle et al. (2017) suggest ~60 mbar, and Batalha et al. (2016) suggest > 1000 mbar (Kite 2019). *Missions:* Mars 2020 will target Jezero crater. The Jezero watershed likely saw surface runoff during both the Late Noachian / Early Hesperian and Hesperian / Amazonian periods (Grant & Golombek 2018). Our work will constrain atmospheric evolution during the Hesperian, and so will help provide long-term global context for inherently local (and likely stratigraphically restricted) sample acquisition by Mars 2020. Our work will complement MAVEN escape-rate data, which is useful but ambiguous due to the uncertain source of escaping O (CO_2 or H_2O), among other factors (Jakosky et al. 2018, Lillis et al. 2017, Ramstad et al. 2018). The proposed work will fill a crucial gap in temporal coverage (Fig. 8), and is directly tied to the geologic record of rivers and lakes.

2.6 Work Plan.

	Activities/milestones	Deliverables
Year 1	• Incorporate gray gas absorber into MarsWRF. • Begin construction of the MarsWRF look-up table. • Train Graduate Student Researcher on MarsWRF analysis. • Compare first-cut GCM output to data for two geologic epochs.	►LPSC presentation on: gray gas results. ►Short GRL-length manuscript on: first-cut reconstruction of P_{CO2} for LN/EH and LH/A geologic epochs.
Year 2	• Complete assembly of the MarsWRF look-up table. • Refine geologic data by sub-dividing Collaborator Morgan's Late Hesperian / Amazonian dataset into two on the basis of crater-retention age. • Begin comparison to geologic data.	►LPSC presentation on: MarsWRF look-up table. ►Detailed (JGR-length) manuscript on: Cause, and P_{CO2} threshold, for the shift in surface liquid water locations with increasing P_{CO2} .
Year 3	• Complete parameter sweeps using the GCM. Confront the results with geologic data for four geologic epochs. Compute P_{CO2} implications. • Compare elevation+latitude P_{CO2} constraints with other • P_{CO2} constraints in a simple atmosphere-evolution model.	►LPSC presentation on: Data-model comparison. ►Detailed manuscript (PNAS/EPSL-length) including refined data analysis.

From experience gained during prior MarsWRF activities by the co-I (e.g. Mischna & Shirley 2017) and the PI (e.g. Kite et al. 2019b), approximately 4,000 CPU-hours will be required per 7-Mars-year simulation. Therefore, we will require 800,000 CPU-hours for the runs needed. The PI's share of UChicago's 'Midway' cluster easily satisfies all our CPU and storage requirements. Other initial and boundary conditions are varied as specified below. Based on the prior experience of both the PI and the co-I with MarsWRF (Mansfield et al. 2018; Kite et al. 2017b; Mischna & Shirley 2017), time for analysis and interpretation (and not CPU time), sets the length of the project. We set the number of runs, and the number of parameters to vary (Table 1), based on this prior experience. **The proposed work has low implementation risk:** this is because the proposed work represents runs of an existing model; by a team already experienced in that model's use; and has a scale less demanding in terms of number of runs and CPU-hours than work already completed by the same team, with the same model, on the same cluster (Kite et al. 2019b).

2.7 Personnel and Qualifications. (For FTE information, see §6, Table of Work Effort).

PI **Edwin Kite** is an Assistant Professor at the University of Chicago. As PI, he will participate to some degree in all aspects of the proposed work and oversee its implementation. Co-I **Michael Mischna** is the Deputy Chief Scientist of the Solar System Exploration Directorate (a 0.5-FTE role) at JPL, and is the developer of the Early Mars branch of MarsWRF; he will carry out the code modifications, assist with the setup and analysis of the GCM calculations, and help with the analysis of the output. (The PI and Co-I are experienced with setting up and analyzing large ensembles of MarsWRF runs; e.g., Kite et al. 2019b describes results from a 147-MarsWRF-run project). Under Kite's supervision, a **UChicago Graduate Student Researcher** (to be identified) will lead the implementation of the model-data comparison, and will be trained by Kite to analyze the GCM model output. Collaborator **Alexander Morgan** will provide guidance on the use of his global database of Mars fans/deltas. All personnel will participate in interpretation of results.

3. References.

Arvidson, R. E., 2016, Aqueous history of Mars as inferred from landed mission measurements of rocks, soils, and water ice, J. Geophys. Res.: Planets, 121, 1602-1626.

Batalha, N. E.; Kopparapu, Ravi Kumar; Haqq-Misra, Jacob; Kasting, J. F., 2016, Climate cycling on early Mars caused by the carbonate-silicate cycle, Earth Planet. Sci. Lett., 455, 7-13.

Borg, Lars; Drake, M. J., 2005, A review of meteorite evidence for the timing of magmatism and of surface or near-surface liquid water on Mars, J. Geophys. Res.,110,E12, E12S03.

S. Bouley, D. Baratoux, I. Matsuyama, F. Forget, A. Séjourné, M. Turbet, F. Costard, Late Tharsis formation and implications for early Mars. Nature 531(7594), 344–347 (2016)

Bristow, T. F.; Haberle, R. M.; Blake, D. F.; et al., 2017, Low Hesperian PCO_2 constrained from in situ mineralogical analysis at Gale Crater, Mars, Proc. Natl. Acad. Sci. : 114 : 9 2166-2170.

Caldeira, Ken; Bala, Govindasamy; Cao, Long, 2013, The Science of Geoengineering, Annual Review of Earth and Planetary Sciences, vol. 41, pp. 231-256.

Carr, M. H., 2006, The Surface of Mars, Cambridge University Press, Cambridge, UK.

Cassata, W. S.; Shuster, D. L.; Renne, P. R.; Weiss, B. P., 2012, Trapped Ar isotopes in meteorite ALH 84001 indicate Mars did not have a thick ancient atmosphere, Icarus, 221, 1, 461-465.

Cawley, Jon C.; Irwin, Rossman P., 2018, Evolution of Escarpments, Pediments, and Plains in the Noachian Highlands of Mars, Journal of Geophysical Research: Planets, Volume 123, Issue 12, pp. 3167-3187

Citron, R. I.; Manga, M.; Hemingway, Douglas J., 2018, Timing of oceans on Mars from shoreline deformation, Nature, 555, 7698, 643-646.

Craddock, R. A.; Maxwell, T. A., 1993, Geomorphic evolution of the Martian highlands through ancient fluvial processes, Journal of Geophysical Research (ISSN 0148-0227), vol. 98, no. E2, p. 3453-3468.

Davis, J. M.; Balme, M.; Grindrod, M.; Williams, R. M. E.; Gupta, S., 2016, Extensive Noachian fluvial systems in Arabia Terra: Implications for early Martian climate, Geology, 44, 10, 847-850.

Dundas, Colin M.; Byrne, Shane, 2010, Modeling sublimation of ice exposed by new impacts in the martian mid-latitudes, Icarus, Volume 206, Issue 2, p. 716-728.

Dundas, C.M., McEwen, A.S., Diniega, S., Hansen, C.J., Byrne, S., and J.N. McElwaine, 2017a, The formation of gullies on Mars today, Geological Society, London, Special Publications, 467, https://doi.org/10.1144/SP467.5

Dundas, C.M.; McEwen, Alfred S.; Chojnacki, Matthew; et al., 2017b, Granular flows at recurring slope lineae on Mars indicate a limited role for liquid water, Nature Geoscience, 10, 903-+.

Fassett, C. I.; Head, J. W., 2008a, The timing of martian valley network activity: Constraints from buffered crater counting, Icarus,195,1, 61-89.

Fastook et al., 2008, Tropical mountain glaciers on Mars: Altitude-dependence of ice accumulation, accumulation conditions, formation times, glacier dynamics, and implications for planetary spin-axis/orbital history, Icarus 198, 305-317.

Forget, F.; Wordsworth, R.; Millour, E.; Madeleine, J.-B.; Kerber, L.; Leconte, J.; Marcq, E.; Haberle, R. M., 2013, 3D modelling of the early martian climate under a denser CO_2 atmosphere: Temperatures and CO2 ice clouds, Icarus,222,1, 81-99.

Goddard, Kate; Warner, N. H.; Gupta, Sanjeev; Kim, Jung-Rack, 2014, Mechanisms and timescales of fluvial activity at Mojave and other young Martian craters, J. Geophys. Res.: Planets, 119, 604-634.

Golombek, M. P.; Warner, N. H.; Ganti, V.; Lamb, M. P.; Parker, T. J.; Fergason, R. L.; Sullivan, R. 2014, Small crater modification on Meridiani Planum and implications for erosion rates and climate change on Mars, J. Geophys. Res.: Planets, 119, 2522-2547

Govindasamy, Bala; Caldeira, Ken, 2000, Geoengineering Earth's radiation balance to mitigate CO2-induced climate change, Geophysical Research Letters, Volume 27, Issue 14, p. 2141-2144

Grant, John A.; Golombek, Matthew P.; Wilson, Sharon A.; Farley, Kenneth A.; Williford, Ken H.; Chen, Al, 2018, The science process for selecting the landing site for the 2020 Mars rover, Planetary and Space Science, Volume 164, p. 106-126.

Grotzinger, J. P.; Arvidson, R. E.; Bell, J. F.; Calvin, W.; Clark, B. C.; Fike, D. A.; Golombek, M.; Greeley, R.; Haldemann, A.; Herkenhoff, K. E.; Jolliff, B. L.; Knoll, A. H.; Malin, M.; McLennan, S. M.; Parker, T.; Soderblom, L.; Sohl-Dickstein, J. N.; Squyres, S. W.; Tosca, N. J.; Watters, W. A., 2005, Stratigraphy and sedimentology of a dry to wet eolian depositional system, Burns formation, Meridiani Planum, Mars, Earth Planet. Sci. Lett.,240,1, 11-72.

Grotzinger, J.P., and R.E. Milliken, 2012, The sedimentary rock record of Mars: distribution, origins, and global stratigraphy, in Sedimentary Geology of Mars SEPM Special Publication No. 102, Print ISBN 978-1-56576-312-8, 1–48.

Haberle, R. M.; Catling, D. C.; Carr, M. H.; Zahnle, K. J., 2017, The Early Mars Climate System, in The atmosphere and climate of Mars, Edited by R.M. Haberle et al. ISBN: 9781139060172. Cambridge University Press, 2017, 497-525

Hauber, E.; Platz, T.; Reiss, D.; Le Deit, L.; Kleinhans, M. G.; Marra, W. A.; Haas, T.; Carbonneau, P., 2013, Asynchronous formation of Hesperian and Amazonian-aged deltas on Mars and implications for climate, J. Geophys. Res.: Planets, 118, 1529-1544.

Head, J. W.; Marchant, D. R., 2014, The climate history of early Mars: insights from the Antarctic McMurdo Dry Valleys hydrologic system, Antarctic Science, 26, 06, 774-800, 774

Head, J. W.; Wordsworth, R.; Forget, F.; Turbet, M., 2017, Deciphering the Noachian Geological and Climate History of Mars: Part 2: A Noachian Stratigraphic View of Major Geologic Processes and Their Climatic Consequences, Fourth International Conference on Early Mars: Geologic, Hydrologic, and Climatic Evolution and the Implications for Life, Proceedings of the conference held 2-6 October, 2017 in Flagstaff, Arizona. LPI Contribution No. 2014, 2017, id.3047

Hecht, M. H., 2002, Metastability of Liquid Water on Mars, Icarus, 156, 2, 373-386.

Hoke, Monica R. T.; Hynek, Brian M., 2009, Roaming zones of precipitation on ancient Mars as recorded in valley networks, Journal of Geophysical Research, 114, CiteID E08002.

Howard, A. D.; Moore, J. M.; Irwin, R. P., 2005, An intense terminal epoch of widespread fluvial activity on early Mars: 1. Valley network incision and associated deposits, J. Geophys. Res.,110,E12, E12S14.

Howard, A., 2007, Simulating the development of Martian highland landscapes through the interaction of impact cratering, fluvial erosion, and variable hydrologic forcing, Geomorphology 91, 332-363.

Hynek, B. M.; Beach, M.; Hoke, M. R. T., 2010, Updated global map of Martian valley networks and implications for climate and hydrologic processes, J. Geophys. Res., 115, E9, E09008.

Ingersoll, Andrew P., 1970, Mars: Occurrence of Liquid Water, Science, Volume 168, Issue 3934, pp. 972-973

Irwin, R. P., 2013, Testing Links Between Impacts and Fluvial Erosion on Post-Noachian Mars, 44th Lunar and Planetary Science Conference, held March 18-22, 2013 in The Woodlands, Texas. LPI Contribution No. 1719, p.2958

Jakosky, B.M. et al., 2018, Loss of the Martian atmosphere to space: Present-day loss rates determined from MAVEN observations and integrated loss through time, Icarus, 315, 146-157.

Kasting, James F.; Kopparapu, Ravikumar; Ramirez, Ramses M.; Harman, Chester E., 2014, Remote life-detection criteria, habitable zone boundaries, and the frequency of Earth-like planets around M and late K stars, Proceedings of the National Academy of Sciences, Volume 111, Issue 35, 2014, pp.12641-12646

Kite, E.S., Michaels, T.I., Rafkin, S.C.R., Manga, M., & W.E. Dietrich, 2011a. Localized precipitation and runoff on Mars, J. Geophys. Res. – Planets, 116, E07002, 20 doi:10.1029/2010JE003783.

Kite, E. S.; Rafkin, Scot; Michaels, Timothy I.; Dietrich, William E.; Manga, M., 2011b, Chaos terrain, storms, and past climate on Mars, J. Geophys. Res., 116, E10, E10002

Kite, E. S.; Halevy, Itay; Kahre, Melinda A.; Wolff, M. J.; Manga, M., 2013a, Seasonal melting and the formation of sedimentary rocks on Mars, with predictions for the Gale Crater mound, Icarus,223,1, 181-210.

Kite, E.S., Lucas, A., & C.I. Fassett, 2013b, Pacing Early Mars river activity: Embedded craters in the Aeolis Dorsa region imply river activity spanned ≳(1–20) Myr, Icarus, 225, 850-855.

Kite, E. S.; Williams, J.-P.; Lucas, Antoine; Aharonson, O., 2014, Low palaeopressure of the martian atmosphere estimated from the size distribution of ancient craters, Nature Geoscience, 7, 5, 335-339.

Kite, E. S.; Gao, P.; Goldblatt, C.; Mischna, M. A.; Mayer, D. P.; Yung, Yuk L., 2017a, Methane bursts as a trigger for intermittent lake-forming climates on post-Noachian Mars, Nature Geoscience, 10, 737-740.

Kite, E. S.; Sneed, Jonathan; Mayer, D. P.; Wilson, Sharon A., 2017b, Persistent or repeated surface habitability on Mars during the late Hesperian – Amazonian, Geophys. Res. Lett., 44, 3991-3999

Kite, E.S., 2019, "Geologic constraints on Early Mars climate," Space Science Reviews, 215: 10, https://doi.org/10.1007/s11214-018-0575-5

Kite, E.S., Mayer, D.P., Wilson, S.A., Davis, J.M., Lucas, A.S., & Stucky de Quay, G., 2019a, "Persistence of intense, climate-driven runoff late in Mars history," Science Advances, March issue.

Kite, E.S., Steele, L., & Mischna, M.A., 2019b, "Aridity enables warm climates on Mars," talk presented at 50th Lunar and Planetary Science Conference, abstract at https://www.hou.usra.edu/meetings/lpsc2019/pdf/1360.pdf .

Knoll, A. H.; Jolliff, Brad L.; Farrand, William H.; Bell, J. F., III; Clark, Benton C.; Gellert, R.; Golombek, M. P.; Grotzinger, J. P.; Herkenhoff, K. E.; Johnson, J. R.; McLennan, S. M.; Morris, R.; Squyres, S. W.; Sullivan, R.; Tosca, N. J.; Yen, A.; Learner, Z., 2008, Veneers, rinds, and fracture fills: Relatively late alteration of sedimentary rocks at Meridiani Planum, Mars, J. Geophys. Res., 113, E6, E06S16.

Kraal, Erin R.; Asphaug, Erik; Moore, Jeffery M.; Howard, Alan; Bredt, Adam, 2008a, Catalogue of large alluvial fans in martian impact craters, Icarus, 194, 1, 101-110.

Kurokawa, H.; Kurosawa, K.; Usui, T., 2018, A lower limit of atmospheric pressure on early Mars inferred from nitrogen and argon isotopic compositions, Icarus, 299, 443-459.

Lammer, Helmut; Zerkle, Aubrey L.; Gebauer, Stefanie; Tosi, Nicola; Noack, Lena; Scherf, Manuel; Pilat-Lohinger, Elke; Güdel, Manuel; Grenfell, John Lee; Godolt, Mareike; Nikolaou,

Athanasia, 2018, Origin and evolution of the atmospheres of early Venus, Earth and Mars, The Astronomy and Astrophysics Review, Volume 26, Issue 1, article id. 2, 72 pp.

Lapôtre, M. G. A.; Ewing, R. C.; Lamb, M. P.; et al., 2016, Large wind ripples on Mars: A record of atmospheric evolution, Science, 353 : 6294 55-58.

Leask, E. K.; Ehlmann, B. L.; Dundar, M. M.; Murchie, S. L.; Seelos, F. P., 2018, Challenges in the Search for Perchlorate and Other Hydrated Minerals With 2.1-μm Absorptions on Mars, Geophysical Research Letters, 45, 12180-12189.

Lillis, R. J.; Deighan, J.; Fox, J. L.; Bougher, S. W.; Lee, Yuni; Combi, M. R.; Cravens, T. E.; Rahmati, Ali; Mahaffy, P. R.; Benna, Mehdi; Elrod, M. K.; McFadden, J. P.; Ergun, Robert. E.; Andersson, Laila; Fowler, C. M.; Jakosky, B. M.; Thiemann, Ed; Eparvier, F.; Halekas, J. S.; Leblanc, François; C., Jean-Yves, 2017, Photochemical escape of oxygen from Mars: First results from MAVEN in situ data, J. Geophys. Res.: Space Physics, 122, 3815-3836.

Malin, M. C.; Edgett, K. S., 2000, Sedimentary Rocks of Early Mars, Science, 290, 1927-1937.

Malin, M. C.; Edgett, K. S., 2003, Evidence for Persistent Flow and Aqueous Sedimentation on Early Mars, Science, 302, 5652, 1931-1934.

Malin, M. C.; Edgett, K. S.; Cantor, Bruce A.; Caplinger, M. A.; Danielson, G. Edward; Jensen, Elsa H.; Ravine, M. A.; Sandoval, J. L.; Supulver, Kimberley D., 2010, An overview of the 1985-2006 Mars Orbiter Camera science investigation, Mars: Intl. Journal of Mars Science and Exploration, 4, p.1-60

Manga, M.; Patel, Ameeta; Dufek, Josef; Kite, E. S., 2012, Wet surface and dense atmosphere on early Mars suggested by the bomb sag at Home Plate, Mars, Geophys. Res. Lett., 39, 1, L01202.

Mangold, N., 2012, Fluvial landforms on fresh impact ejecta on Mars, Planet. & Space Sci.,62,1, 69-85.

Mangold, N.; Adeli, S.; Conway, S.; Ansan, V.; Langlais, B., 2012, A chronology of early Mars climatic evolution from impact crater degradation, J. Geophys. Res., 117, E4, E04003.

Mangold, N.; Kite, E. S.; Kleinhans, M. G.; Newsom, H.; Ansan, V.; Hauber, E.; Kraal, E.; Quantin, C.; Tanaka, K., 2012, The origin and timing of fluvial activity at Eberswalde crater, Mars, Icarus, Volume 220, Issue 2, p. 530-551.

Mansfield, Megan; Kite, E. S.; Mischna, M. A., 2018, Effect of Mars Atmospheric Loss on Snow Melt Potential in a 3.5 Gyr Mars Climate Evolution Model, J. Geophys. Res.: Planets, 123,4, 794-806

McEwen, A. S.; Eliason, E. M.; Bergstrom, J. W.; Bridges, N. T.; Hansen, C. J.; Delamere, W. A.; Grant, J. A.; Gulick, V. C.; Herkenhoff, K. E.; Keszthelyi, L.; Kirk, R. L.; Mellon, M. T.;

Squyres, S. W.; Thomas, N.; Weitz, C. M., 2007, Mars Reconnaissance Orbiter's High Resolution Imaging Science Experiment (HiRISE), J. Geophys. Res., 112, E5, E05S02.

Mischna, Michael A.; Richardson, Mark I.; Wilson, R. John; McCleese, Daniel J., 2003, On the orbital forcing of Martian water and CO2 cycles: A general circulation model study with simplified volatile schemes, Journal of Geophysical Research Planets, Volume 108, Issue E6, CiteID 5062, DOI 10.1029/2003JE002051

Mischna, Michael A.; Lee, Christopher; Richardson, Mark, 2012, Development of a fast, accurate radiative transfer model for the Martian atmosphere, past and present, Journal of Geophysical Research, Volume 117, Issue E10, CiteID E10009

Mischna, M. A.; Baker, V.; Milliken, R.; Richardson, M.; Lee, C., 2013, Effects of obliquity and water vapor/trace gas greenhouses in the early martian climate, J. Geophys. Res.: Planets,118,3, 560-576

Mischna, Michael A.; Shirley, James H., 2017, Numerical modeling of orbit-spin coupling accelerations in a Mars general circulation model: Implications for global dust storm activity, Planetary and Space Science, Volume 141, p. 45-72.

Morgan, A. M.; Wilson, S. A.; Howard, A. D.; Craddock, R. A.; Grant, J. A., 2018, Global Distribution of Alluvial Fans and Deltas on Mars, 49th Lunar and Planetary Science Conference 19-23 March, 2018, held at The Woodlands, Texas LPI Contribution No. 2083, id.2219

Niles, B.; Michalski, Joseph; Ming, Douglas W.; Golden, D. C., 2017, Elevated olivine weathering rates and sulfate formation at cryogenic temperatures on Mars, Nature Communications, 8, id. 998.

Moore, Jeffrey M.; Howard, Alan D., 2005, Large alluvial fans on Mars, Journal of Geophysical Research, Volume 110, Issue E4, CiteID E04005

Palumbo, Ashley M.; Head, James W., 2018, Early Mars Climate History: Characterizing a "Warm and Wet" Martian Climate With a 3-D Global Climate Model and Testing Geological Predictions, Geophysical Research Letters, 45, 10249 -

Palumbo, Ashley M.; Head, James W.; Wordsworth, Robin D., 2018, Late Noachian Icy Highlands climate model: Exploring the possibility of transient melting and fluvial/lacustrine activity through peak annual and seasonal temperatures, Icarus, Volume 300, p. 261-286.

Pielke, R., 2002, Mesoscale meteorological modeling, 2nd edition.

Ramstad, Robin; Barabash, Stas; Futaana, Yoshifumi; Nilsson, Hans; Holmström, Mats, 2018, Ion Escape From Mars Through Time: An Extrapolation of Atmospheric Loss Based on 10 Years of Mars Express Measurements, Journal of Geophysical Research: Planets, 123, 3051-3060.

Ramirez, R. M.; Craddock, R. A., 2018, The geological and climatological case for a warmer and wetter early Mars, Nature Geoscience, 11, 4, 230-237

Richardson, Mark I.; Wilson, R. John, 2002, Investigation of the nature and stability of the Martian seasonal water cycle with a general circulation model, Journal of Geophysical Research (Planets), Volume 107, Issue E5, CiteID 5031, DOI 10.1029/2001JE001536

Richardson, Mark I.; Toigo, Anthony D.; Newman, Claire E., 2007, Investigation of the nature and stability of the Martian seasonal water cycle with a general circulation model, Journal of Geophysical Research, vol. 112, issue E9, p. E09001 (2007)

Sagan, Carl; Toon, O. B.; Gierasch, P. J., 1973, Climatic Change on Mars, Science, Volume 181, Issue 4104, pp. 1045-1049

Skamarock, W. C., J. B. Klemp, J. Dudhia, D. O. Gill, D. M. Barker, W. Wang, and J. G. Powers, 2005: A Description of the Advanced Research WRF Version 2. NCAR Technical Note NCAR/TN-468+STR, doi:10.5065/D6DZ069T.

Soto, Alejandro; Mischna, Michael; Schneider, Tapio; Lee, Christopher; Richardson, Mark, 2015, Martian atmospheric collapse: Idealized GCM studies, 2015, Icarus, Volume 250, p. 553-569.

Sullivan, Robert; Greeley, Ronald; Kraft, Michael; Wilson, Gregory; Golombek, Matthew; Herkenhoff, Ken; Murphy, James; Smith, Peter, 2000, Results of the Imager for Mars Pathfinder windsock experiment, Journal of Geophysical Research, Volume 105, Issue E10, p. 24547-24562

Tarter, Jill C.; Backus, Peter R.; Mancinelli, Rocco L.; Aurnou, Jonathan M.; Backman, Dana E.; Basri, Gibor S.; Boss, Alan P.; Clarke, Andrew; Deming, Drake; Doyle, Laurance R.; Feigelson, Eric D.; Freund, Friedmann; Grinspoon, David H.; Haberle, Robert M.; Hauck, Steven A., II; Heath, Martin J.; Henry, Todd J.; Hollingsworth, Jeffery L.; Joshi, Manoj M.; Kilston, Steven; Liu, Michael C.; Meikle, Erik; Reid, I. Neill; Rothschild, Lynn J.; Scalo, John; Segura, Antigona; Tang, Carol M.; Tiedje, James M.; Turnbull, Margaret C.; Walkowicz, Lucianne M.; Weber, Arthur L.; Young, Richard E., 2007, A Reappraisal of The Habitability of Planets around M Dwarf Stars, Astrobiology, Volume 7, Issue 1, pp. 30-65.

Tian, Feng; Kasting, James F.; Solomon, Stanley C., 2009, Thermal escape of carbon from the early Martian atmosphere, Geophysical Research Letters, Volume 36, Issue 2, CiteID L02205.

Tanaka, K. L.; Robbins, S. J.; Fortezzo, C. M.; Skinner, J. A.; Hare, T. M., 2014, The digital global geologic map of Mars, Planet. & Space Sci., 95, 11-24.

Tornabenw et al. 201X

Tosca, N.J., Imad A. M. Ahmed, Benjamin M. Tutolo, Alice Ashpitel & Joel A. Hurowitz, Magnetite authigenesis and the warming of early Mars, Nature Geoscience, 11, 635–639.

Tu, Lin; Johnstone, Colin P.; Güdel, Manuel; Lammer, Helmut, 2015, The extreme ultraviolet and X-ray Sun in Time: High-energy evolutionary tracks of a solar-like star, Astronomy & Astrophysics, Volume 577, id.L3, 4 pp.

Turbet, M.; Tran, H., 2017, Comment on "Radiative Transfer in CO2-Rich Atmospheres: 1. Collisional Line Mixing Implies a Colder Early Mars", J. Geophys. Res.: Planets, 122, 2362-2365.

Urata, Richard A.; Toon, Owen B., 2013, Simulations of the martian hydrologic cycle with a general circulation model: Implications for the ancient martian climate, Icarus, 226, 1, 229-250.

Warner, Nicholas H.; Gupta, Sanjeev; Calef, Fred; Grindrod, Peter; Boll, Nathan; Goddard, Kate, 2015, Minimum effective area for high resolution crater counting of martian terrains, Icarus, 245, 198-240.

Warren, A.O., & Kite, E.S., "A new Martian paleopressure constraint before 4 Ga from crater size-frequency distributions in Mawrth Vallis," for presentation at 50th Lunar and Planetary Science Conference

Williams, R. M. E.; Phillips, R. J., 2001, Morphometric measurements of martian valley networks from Mars Orbiter Laser Altimeter (MOLA) data, J. Geophys. Res., 106, E10, 23737-23752.

Williams, R. M. E.; Malin, M. C., 2008, Sub-kilometer fans in Mojave Crater, Mars, Icarus,198,2, 365-383.

Wilson, S. A.; Howard, A. D.; Moore, J. M.; Grant, J.A., 2016, A cold-wet middle-latitude environment on Mars during the Hesperian-Amazonian transition: Evidence from northern Arabia valleys and paleolakes, J. Geophys. Res.: Planets, 121, 1667-1694.

Wordsworth, R.; Forget, F.; Millour, E.; Head, J. W.; Madeleine, J.-B.; Charnay, B., 2013, Global modelling of the early martian climate under a denser CO2 atmosphere: Water cycle and ice evolution, Icarus, 222, 1-19.

Wordsworth, R. D.; Kerber, L.; Pierrehumbert, R. T.; Forget, F.; Head, J. W., 2015, Comparison of "warm and wet" and "cold and icy" scenarios for early Mars in a 3-D climate model, J. Geophys. Res.: Planets, 120,6, 1201-1219.

Wordsworth, Robin D., 2016, The Climate of Early Mars, Annual Rev. Earth Planet. Sci., 44, p.381-408

Zalucha, Angela M.; Plumb, R. Alan; Wilson, R. John, 2010, An Analysis of the Effect of Topography on the Martian Hadley Cells, Journal of the Atmospheric Sciences, vol. 67, issue 3, pp. 673-693

4. Data Management Plan (maximum 2 pages).

NASA Planetary Science Division ROSES Data Management Plan (DMP) Template

Proposers should to refer to the following documents in preparing DMPs:

- ROSES progam element C.1, Section 3.6.1
- Planetary Science Division FAQ for Data Management Plans (which will appear under "other documents" on NSPIRES pages in Appendix C)
- NASA Plan for increasing access to results of Federally funded research

1. Overview of the data that will be produced by the proposed project:

The main data needed to reproduce our results are the maps of surface temperature and water ice stability for each of our <250 GCM runs.

2. Data types, volume, formats, and (where relevant) standards:

Input: MarsWRF-ingestible plain text, negligible size. Output: .ctl and .dat files, GrADS format, totaling ~1 GB. (This is for a fairly comprehensive output file with almost all microphysics variables output). <250 runs, so total <250 GB of output for the entire input and output files.

3. Schedule for data archiving and sharing:

Data will be uploaded within 3 months of the publication of the corresponding paper.

4. Intended repositories for archived data and mechanisms for public access and distribution:

In addition to releasing the required minimal data in supplementary materials along with publications, the complete output from the final year of selected GCMs calculations will be uploaded in the widely used Grid Analysis and Display System (GrADS) format to archive https://its.uchicago.edu/uchicago-box/ by the end of the award. It is not practical (due to the large size of the output files) to upload every time-snapshot from the GCM output for all GCM runs, therefore annual averages for all parameters will be made available. The University of Chicago archive complies with NASA's requirement for a "stable and long-term supported data repository." The PI has experience with this archive. For example, the University of Chicago archive will be the location for public sharing of ~1 TB of Kite-lab stereo DTMs. Uploading of data and appropriate README files will be carried out by the PI. ~3% of the PI's time (i.e., 0.5 weeks total) is allocated for this task; because the archive already exists, this is sufficient.

5. Plan for enabling long-term preservation of the data:

The University of Chicago archive complies with NASA's requirement for a "stable and long-term supported data repository."

6. Software archiving plan:

The core MarsWRF (and PlanetWRF, and WRF) code on which our work is based is available from the developers, who can supply instructional support only on a best-effort basis. According to Appendix C of ROSES, "Stand-alone code that is not straightforward to implement or whose utility is significantly outweighed by the costs to share it is not expected to be made available," therefore, we do not plan to put our improved branch of MarsWRF on Github.

7. Astromaterials archiving plan:

Not applicable.

8. Roles and responsibilities of team members for data management:

The PI will be responsible for uploading the files from the University of Chicago cluster to the University of Chicago data archive. The PI will also be responsible for writing a README file to explain the contents of the archive.